

OrchestrRL: Dynamic Compute and Network Orchestration for Disaggregated RL

Xin Tan¹, Yicheng Feng¹, Yu Zhou², Yimin Jiang², Yibo Zhu², Hong Xu¹
¹The Chinese University of Hong Kong, ²StepFun

Abstract

Disaggregating the generation and training stages in RL is widely adopted to scale LLM post-training. There are two critical challenges here. First, the generation stage often becomes a bottleneck due to dynamic workload shifts and severe execution imbalances. Second, the decoupled stages result in diverse and dynamic network traffic patterns that strain the conventional static fabric.

We build OrchestrRL to orchestrate dynamically both compute and network in disaggregated RL. OrchestrRL employs an adaptive compute scheduler that adjusts parallelism configuration to match changing workload characteristics within and across generation steps. OrchestrRL adopts a reconfigurable optical-electrical fabric called RFabric: It leverages optical circuit switches to reconfigure the aggregation and core layers of the topology on demand, tailoring bandwidth resources to the unique communication patterns across various phases of training, generation, and weight synchronization. Evaluated on a 64-H800 GPU testbed, OrchestrRL demonstrates up to a 1.42× throughput improvement over static baselines. Using a high-fidelity simulator, we also show that RFabric achieves superior performance-cost efficiency at scale over static Fat-Tree networks.

1 Introduction

Reinforcement Learning (RL) has emerged as a pivotal post-training technique, enabling instruction-following and reasoning capabilities for large language models (LLMs) [3, 4, 39]. The RL workflow differs from pre-training. For each data batch, it alternates between two stages: sample generation (roll-out) and model training. Generation is memory- and bandwidth-bound since it is autoregressive inference. Training is compute-bound: it evaluates those sample responses to compute gradients and update model weights.

This workflow has two defining characteristics: (1) a strict data dependency that training must wait for generation to complete, and (2) divergent resource requirements across the stages. State-of-the-art RL frameworks [35, 57, 67] adopt a disaggregated architecture, using specialized GPU clusters for each stage and enabling asynchronous execution, where generation runs with slightly stale model weights. Although fully asynchronous execution has been explored [35, 56], this work focuses on the widely adopted *one-step asynchronous* setting [50, 57, 67], which offers a practical balance between algorithmic stability and system throughput.

Despite its benefits, disaggregation suffers from two primary inefficiencies that limit performance and scalability. First, generation often becomes the end-to-end bottleneck due to rapidly shifting workloads and load imbalance. Within a single step, the workload evolves from many short generations to a long tail of a small number of lingering responses; across steps, response length distributions can drift as training progresses. As a result, an efficient parallelism configuration at the early stage can become suboptimal later, and stragglers can dominate the step makespan (§2). These effects are amplified by unpredictable output lengths and varying KV-cache demands, which cause some GPUs to be underutilized while others are overloaded. Unlike online serving that optimizes metrics such as Time-to-First-Token (TTFT), RL generation is an offline batched workload where the objective is to minimize the *step makespan*—time to complete all samples in a generation step. However, existing RL systems largely rely on static or manually tuned parallelism strategies [35, 57, 67], which are poorly suited to these intra-step and inter-step dynamics.

The second inefficiency lies in a mismatch with the network fabric. Training and generation stages impose diverse and intense traffic patterns. Training requires high bisection bandwidth for efficient collective communications (e.g., all-reduce for Data Parallelism (DP), all-to-all for Expert Parallelism (EP) and all-gather/reduce-scatter for Tensor Parallelism (TP)) which alternates within each training iteration. Generation clusters, on the other hand, exhibit bipartite communication patterns, such as M2N traffic from Attention-FFN Disaggregation (AFD) [62, 69] and all-to-all for EP. Disaggregated RL further incurs periodic weight synchronization between training and generation clusters, which is highly bursty. Optical Circuit Switching (OCS) [43, 46, 63] has been recently explored to enable dynamic network topologies that potentially overcome the prohibitive cost and poor utilization of a fixed fabric for dynamic traffic (§2). Yet, current proposals focus on pre-training and fail to consider the distinct traffic demands at the generation stage, highlighting a critical gap that must be addressed to achieve scalable and efficient network fabric for end-to-end RL workflow.

In this work, we present OrchestrRL, a novel orchestration system for disaggregated RL that treats *reconfiguration* as a first-class principle to jointly optimize compute and network.

For mitigating the compute bottleneck, OrchestrRL reconfigures the parallelism strategy in response to workload

shifts and imbalance during generation. As workload characteristics (e.g., batch size and the generation-length distribution) evolve within and across steps, the optimal operating point on the concurrency-latency trade-off shifts. Thus in OrchestrRL a proactive planner runs periodically, identifies the best parallelism configuration (e.g., TP, EP, and AFD with different degrees) that minimizes the expected makespan for the remaining requests, and commits the parallelism change to realign deployment with the current workload. Complementing this, a reactive balancer continuously monitors worker load and performs request migrations to reduce stragglers caused by unpredictable output lengths.

On the networking side, OrchestrRL employs RFabric, a hybrid network fabric tailored to the spatiotemporal dynamics of disaggregated RL. RFabric partitions training and generation resources into distinct Points-of-Delivery (PoDs) and dynamically reallocates bandwidth based on real-time communication patterns. Its hierarchical hybrid optical-electrical design comprises three layers: (i) intra-PoD fabrics using electronic Top-of-Rack switches and OCS-based aggregation, and (ii) an OCS-based core layer interconnecting PoDs. For training PoDs, RFabric configures high-bandwidth topologies to support intensive collective operations that alternate with model layers (e.g., expert parallelism for MoE and context parallelism for Attention) and training phases (forward, backward and gradient synchronization). For generation PoDs, it optimizes for unique bipartite or localized communication patterns. During model synchronization, RFabric temporarily reconfigures the aggregation and core OCS layers to instantiate a two-level, tree-style dissemination overlay from training PoDs to generation PoDs. Crucially, the available slack for hiding circuit reconfiguration overhead varies across stages. RFabric adapts its reconfiguration granularity—reconfiguring when slack permits and avoiding the critical path otherwise—to deliver consistently high performance.

To evaluate OrchestrRL, we conduct experiments on a 64-GPU NVIDIA H800 testbed and build RLSim, a high-fidelity simulator for large-scale studies. On the testbed, OrchestrRL improves end-to-end training throughput by up to 1.42× over existing schemes. At scale, simulations show that RFabric matches the performance of an ideal non-blocking Fat-tree while improving cost-efficiency by 1.53×–2.06×. Moreover, RFabric outperforms prior optical designs [46, 63] and achieves a better performance-cost Pareto frontier.

We make the following contributions.

- We systematically characterize the workload dynamics in disaggregated RL, uncovering generation bottlenecks caused by evolving workload shifts and the mismatch between static network and diverse traffic patterns of training and generation stages and their interaction.
- We propose OrchestrRL, which optimizes compute and network in disaggregated RL via reconfiguration. OrchestrRL

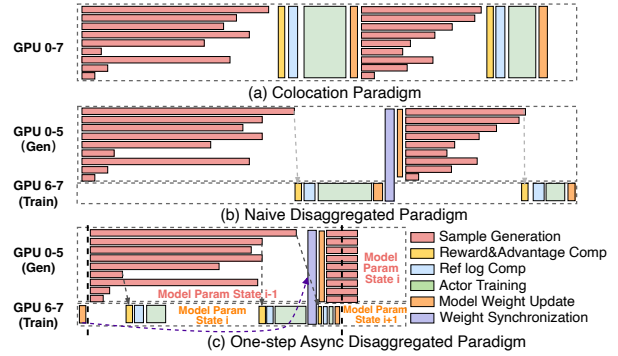


Figure 1: RL workflow in various paradigms with GRPO [55].

includes (i) a compute scheduler that minimizes per-step makespan through dynamic parallelism switching and on-line load rebalancing, and (ii) RFabric, a hierarchical hybrid optical–electrical fabric that enables on-demand topology materialization for stage-specific communication.

- We evaluate OrchestrRL’s compute scheduler on a 64-GPU testbed and evaluate RFabric via large-scale simulation. Results show that OrchestrRL improves training throughput and that RFabric achieves higher cost-efficiency than existing network fabrics.

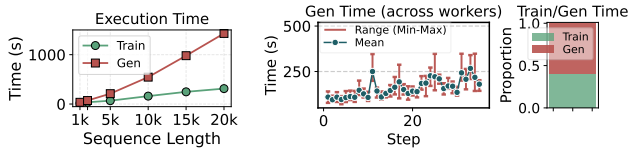
2 Disaggregated RL Workloads

RL systems have evolved from a co-located design to disaggregation. In co-location as in Figure 1(a) [42, 57], memory-bound generation (Gen) and compute-bound training (Train) share the same GPU bundle, and their mismatched resource demands limit utilization and scalability. Naive disaggregation (Figure 1(b)) enables specialized, independently scalable clusters, but synchronous execution creates significant pipeline bubbles. One-step asynchronous disaggregation (Figure 1(c)) [50, 57, 67] overlaps clusters on different batches, reducing bubbles and improving throughput, at the cost of using a one-step-stale policy for Gen.

Here we present a detailed characterization of disaggregated RL workloads with veRL [57] under the prevalent one-step off-policy configuration. Unless otherwise noted, we evaluate a Qwen-2.5 14B model with GRPO on the open1-math-220k dataset [7] over 72 H800 GPUs: a 32-GPU Train cluster and a 40-GPU Gen cluster. Train uses Megatron-LM [6] with Pipeline Parallelism (PP)=2, DP=2 and TP=8, while the Gen side runs vLLM [44] with TP=8 and DP=5.

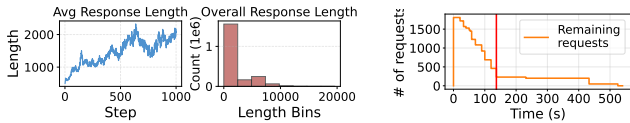
2.1 Generation as a Bottleneck

Gen on the critical path. The Gen stage is far more sensitive to increase in sequence length than Train. As shown in Figure 2a, training and generation have distinct performance profiles. Train, which involves full forward and backward passes on large batches, is predominantly compute-bound,



(a) Execution times (b) Gen worker time profiles. The w.r.t. sequence length; long tail of samples increases skew. batch size 512.

Figure 2: Effect of sequence length on performance.



(a) Distribution of response lengths with a heavy tail. (b) Remaining request number in a Gen step.

Figure 3: Generation dynamics shaped by request completion and length variability.

making it well-suited for modern accelerators. In contrast, Gen is memory bandwidth-constrained and depends on an iterative decoding process, heavily impacted by sequence length. Consequently, Gen frequently dominates the step makespan, taking $1.49\times$ longer than Train in our workload (Figure 2b) on average. This gap can persist even with additional Gen resources, because Gen acts as the producer and its cost scales directly with sequence length.

Root causes of inefficiency. (1) Heavy-tailed and evolving response length distribution, as shown in Figure 3a. Most responses are of moderate length (under 7.5K tokens), but a small fraction of stragglers require substantially more decoding steps and can delay overall processing (Figure 3b), consistent with observations in [67, 68]. (2) Fixed parallelism for changing workloads. Static configurations cannot adapt to shifts in batch size or response length, leading to suboptimal performance. Even within a single generation step, the best parallelism configuration can change across phases under a fixed 8-GPU budget (with $TP \times DP$ constant and batch size 512). We select two snapshots within the step: in the early phase, the step completes fastest with $TP=2$ (79.2s, vs. 96.3s/138.7s for $TP=4/8$), while in the tail phase it is fastest with $TP=8$ (165.1s, vs. 188.3s/208.4s for $TP=4/2$). Clearly, any single fixed configuration is inefficient across the step. (3) Imbalance across workers due to response length variability. As shown in Figure 2b, workers handling shorter responses finish earlier, while those processing longer responses become stragglers (with the max-to-min average time ratio reaching $1.58\times$ in the sampled workload). Additionally, KV cache utilization is also skewed across workers.

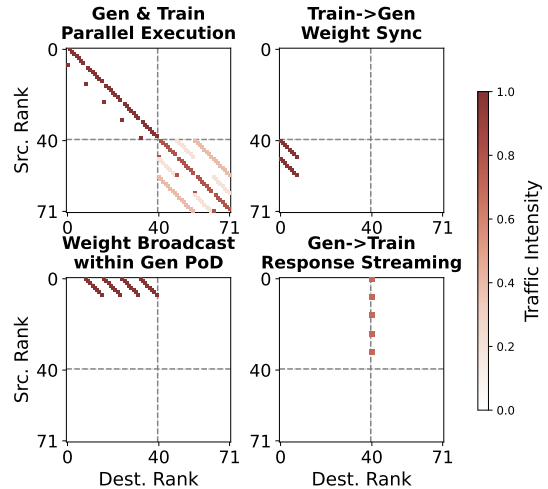


Figure 4: Spatial network traffic across RL stages. For weight synchronization, we use an optimized two-stage scheme: the Train DP group transmits weights once to the DP-0 group of each Gen pod, after which each Gen DP-0 broadcasts locally to its DP peers.

2.2 Asymmetric and Bimodal Traffic

Spatial heterogeneity. Communication is highly asymmetric across stages during concurrent Gen and Train execution (Figure 4). The Train cluster (Ranks 40–71) exhibits structured collective patterns spanning multiple parallelism dimensions: frequent TP all-reduces within model-parallel groups, DP gradient synchronization across DP replicas, and PP send/rcv traffic between adjacent pipeline stages (and, if in MoE (Mixture-of-Experts) settings, additional EP all-to-all exchanges). In contrast, the Gen cluster (Ranks 0–39) communicates almost entirely within small, disjoint TP groups, with negligible traffic across groups. Cross-cluster traffic is sparse and bursty, occurring mainly at stage boundaries for weight synchronization, plus small messages from Gen to Train to stream generated samples back for training.

Temporal heterogeneity and reconfiguration slack. Communication timing and intensity vary across stages, creating intermittent *slack* windows for OCS reconfiguration. We define *communication slack* for a collective event e_k as $\Delta t_k = t_{\text{start}}(e_k) - t_{\text{end}}(e_{k-1})$, the time since the previous communication event. Figure 5 shows that slack is highly heterogeneous with a bimodal distribution.

One mode corresponds to dense phases dominated by model-parallel collectives, where slack remains consistently small, leaving little room for disruption. For example, during Gen, TP collectives occur almost back-to-back, with a median slack below 0.5ms, owing to small inputs and short compute intervals. During Train, TP/PP/DP collectives are still frequent, but longer compute kernels open up larger slack windows (typically tens to hundreds of milliseconds), allowing reconfiguration to be scheduled more judiciously.

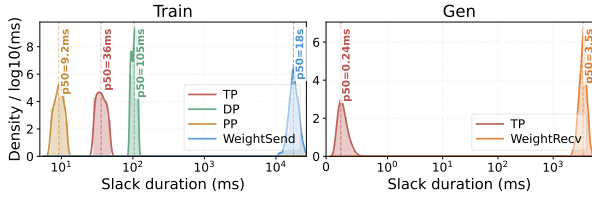


Figure 5: Distribution of slack durations across communication operation types.

The other mode corresponds to sparse weight synchronization (WeightSend/WeightRecv), where events are separated by long idle periods (seconds or more), providing ample opportunities for reconfiguration.

2.3 Design Opportunities

Our analysis highlights two defining characteristics of disaggregated RL. First, the Gen stage (the workflow producer) is highly sensitive to response-length variability, leading to dynamic workload shifts and intra-cluster load imbalance. Second, network demand varies substantially across Train, Gen, and weight synchronization, and changes over time.

Opportunity 1: Adaptive compute scheduling. To adapt to evolving workloads, it is essential to periodically reevaluate parallelism strategies and resource placement for longer-term changes (e.g., batch size and generation length distributions). Further, dynamic request migration can correct short-term imbalances with low overhead. Together, these two operate at different timescales to sustain high utilization.

Moreover, unlike online serving that prioritizes latency (i.e. TTFT) through the prefill-decode trade-offs, generation in RL reasoning is makespan-oriented. In this context, decoding dominates the critical path during long rollouts, shifting the optimization focus to decoding-centric parallelism with less emphasis on prefill-decoding disaggregation [66].

Opportunity 2: Workload-aware network reconfiguration. As shown earlier, disaggregated RL exhibits stage- and parallelism-dependent communication patterns, and our adaptive parallelism (Opportunity 1) further changes collective membership and shifts hotspots over time. This creates a dilemma: Train benefits from high-bandwidth circuits for bulk-synchronous collectives and periodic Train-Gen synchronization, whereas Gen demands sub-millisecond, always-on connectivity for latency-critical fine-grained traffic.

A monolithic fabric struggles to satisfy both requirements. An optical network can provide high and reconfigurable bandwidth. While commodity OCS devices can switch in tens of milliseconds (Table 2), the *end-to-end* time before new links are usable is often dominated by system effects (e.g., clock/data recovery, control-plane actions, and routing updates). For example, MixNet [46] reports OCS control latencies of tens of milliseconds, yet observes multi-second

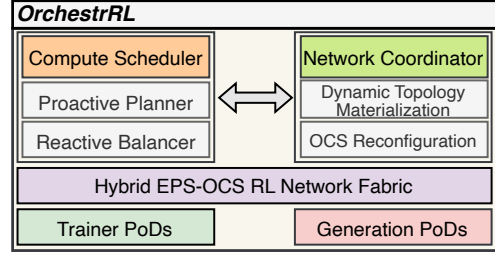


Figure 6: Overview of OrchestrRL.

overheads due to host-side device initialization when the NIC is *directly connected* to the OCS. If such reconfiguration lies on Gen’s critical path, it would dramatically inflate overall latency and degrade performance. Conversely, relying solely on an electrical network forces the fabric to provision for worst-case global traffic, which is costly and still prone to congestion under bursty demand.

These observations motivate RFabric: a hybrid EPS–OCS design that keeps an always-on, host-facing EPS substrate for latency-sensitive traffic, while using an upper-tier OCS to opportunistically provision stage-specific high-bandwidth circuits when slack permits. By aligning circuit schedules with each stage’s dominant communication (e.g., Train forward/backward collectives vs. gradient synchronization), RFabric improves utilization and end-to-end performance under a fixed hardware budget. Moreover, because slack varies widely across stages, RFabric adapts its reconfiguration frequency accordingly.

3 OrchestrRL Overview

OrchestrRL dynamically orchestrates both compute and network resources for disaggregated RL. As shown in Figure 6, OrchestrRL combines a co-designed compute–network architecture with a unified control plane.

Disaggregated PoDs, reconfigurable fabric. OrchestrRL adopts a disaggregated design that partitions training and generation resources into distinct PoDs, enabling specialization and independent scaling. On top of this architecture, OrchestrRL deploys a reconfigurable hybrid optical–electrical fabric (§5.1) that adapts its topology to the stage-dependent communication demands of RL.

Dynamic orchestration. The unified control plane jointly coordinates compute and network to reduce bottlenecks and improve efficiency. *On the compute side*, an adaptive scheduler tracks Gen workloads, adjusts parallelism configurations, and mitigates stragglers via lightweight request migration across replicas to reduce the Gen step makespan (§4). *On the network side*, a workload-aware coordinator translates *workflow intents* (across Train, Gen, and weight synchronization) into topology and bandwidth decisions and reconfigures the fabric on demand (§5).

Algorithm 1 Orchestration for Gen

```

1: Event 1: Periodic proactive planning within each Gen step:
   # Global planning for slow-evolving workload shifts.
2:  $\mathcal{R} \leftarrow \text{cluster.GetPendingReqs}()$ ;  $C_{cur} \leftarrow \text{cluster.GetConfig}()$ 
3:  $Obj_{cur} \leftarrow \text{EstMakespan}(\mathcal{R}, C_{cur})$ 
4:  $\{C_{new}, Obj_{new}, cost\} \leftarrow \text{SolveOptim}(\mathcal{R}, C_{cur})$  ▷ Solve Eq. 1
5: if  $Obj_{new} + cost < Obj_{cur} - \epsilon$  then ▷ Gain is sufficient
6:    $\text{cluster.Reconfigure}(C_{new})$ 

7: Event 2: On each monitoring tick between proactive cycles:
   # Handle transient imbalance under the current configuration.
8:  $\mathcal{L} \leftarrow \text{cluster.GetLoadIndices}()$ 
9:  $\mathcal{R} \leftarrow \text{cluster.GetPendingReqs}()$ 
10: if  $\text{Imbalance}(\mathcal{L}) > \theta$  then
11:    $M \leftarrow \text{IdentifyMigrationCandidates}(\mathcal{L}, \mathcal{R})$ 
12:    $\text{cluster.ExecBalance}(M)$  ▷ Request-state migration

```

4 Dynamic Compute Orchestration

This section describes OrchestrRL’s adaptive compute orchestration. To handle the workload shifts and intra-cluster imbalance identified in §2, OrchestrRL employs a two-level mechanism as summarized in Algorithm 1.

- **Coarse-grained proactive planning** (§4.1): In each Gen step, OrchestrRL periodically forecasts the remaining workload, computes the best parallelism configuration that minimizes the makespan, and updates the deployment if beneficial, in order to adapt to the evolving workload shifts.
- **Fine-grained reactive balancing** (§4.2): On a shorter timescale, OrchestrRL also continuously migrates requests away from stragglers to mitigate the transient imbalances caused by unpredictable workload variations.

4.1 Proactive Planning

During each Gen step, we monitor request progress and assess whether reconfiguring the parallelism can reduce the expected completion time of pending requests. Rather than predicting per-request output lengths—which is both impractical and challenging [52, 67]—we maintain an online estimate of the *step-level* remaining-workload histogram. At the beginning of each step, we forecast this histogram using an ARIMA model [31] trained on output-length statistics from recent steps. As requests are completed, this distribution is dynamically updated by removing finished requests. With the updated distribution and per-request generation progress, we estimate the remaining decoding workload. Accounting for KV-cache constraints, we select the parallelism configuration that minimizes the makespan of the remaining work, and apply it only when the expected gains outweigh reconfiguration overheads.

Problem formulation. Let \mathcal{R} be the set of pending requests and \mathcal{K} the set of *logical instances*. Each instance $k \in \mathcal{K}$ represents a schedulable deployment option: a feasible GPU group together with a parallelism configuration $y_k \in \mathcal{Y}$ (e.g.,

TP/EP/AFD and degree), which uses $G(y_k)$ GPUs. We decide a request-to-instance assignment $\mathbf{X} = [x_{ik}] \in \{0, 1\}^{|\mathcal{R}| \times |\mathcal{K}|}$ and the per-instance configuration vector $\mathbf{Y} = [y_k]$. For instance k , $\mathcal{R}_k(\mathbf{X}) = \{i \in \mathcal{R} : x_{ik} = 1\}$ denotes the requests assigned to it. We denote the current setting as $(\hat{\mathbf{X}}, \hat{\mathbf{Y}})$.

$$\min_{\mathbf{X}, \mathbf{Y}} \max_{k \in \mathcal{K}} \left(T_k(\mathcal{R}_k, y_k) + C_k^{\text{mig}}(\mathbf{X}, \hat{\mathbf{X}}) + C_k^{\text{sw}}(y_k, \hat{y}_k) \right) \quad (1)$$

$$\text{s.t.} \quad \left| \frac{\sum_{i \in \mathcal{R}} x_{ik} \cdot D^{\text{kv}}(i)}{\text{Cap}^{\text{kv}}(y_k)} - \mu \right| \leq \delta, \quad \forall k \in \mathcal{K}, \quad (2)$$

$$\sum_{k \in \mathcal{K}} G(y_k) \leq G_{\text{total}}, \quad (3)$$

$$\sum_{k \in \mathcal{K}} x_{ik} = 1, \quad \forall i \in \mathcal{R}. \quad (4)$$

The objective (1) minimizes the predicted makespan across instances, while accounting for state-migration cost C^{mig} for transferring KV-cache and parallel-mode switching cost C^{sw} . $T_k(\mathcal{R}_k, y_k)$ estimates the remaining completion time of instance k under configuration y_k , capturing batching effects and KV-cache dynamics. Constraint (2) balances KV-cache load *normalized by capacity* by keeping each instance’s KV utilization, $\sum_i x_{ik} D^{\text{kv}}(i) / \text{Cap}^{\text{kv}}(y_k)$, within $\mu \pm \delta$; transient overflows are spilled to CPU memory. Constraint (3) enforces the total GPU budget G_{total} , and (4) assigns each request to exactly one instance.

Reconfiguration and state migration costs. Before discussing how to solve this optimization (1), we ought to take a close look at the overheads of reconfiguring parallelism, C^{sw} and C^{mig} . Executing a new plan takes two steps: updating instance placement and migrating request state. First, model weights need to be re-sharded (and loaded if necessary) according to the new parallel layout. We estimate the this switching cost C^{sw} from the amount of weights to redistribute/reload and the offline-profiled bandwidth/latency of the transfer path. When supported, we also use GPU virtual memory to pre-map (warm up) weight and KV-cache regions for standby configurations to reduce switch-over latency [10], and include this overhead in C^{sw} . Next, KV cache migration to the new sharding scheme is performed via either (1) direct transfer using intra-node NVLink/PCIe and inter-node RDMA, or (2) recomputation by replaying the forward pass from cached token IDs. The migration cost C^{mig} is estimated by comparing KV transfer time with recomputation time, selecting the cheaper option based on an offline-profiled cost model (see Appendix A for details).

Solving the optimization. The optimization program (1) involves a search space of combinations of parallel modes and instance groups which also grow with the number of GPUs and pending requests and is expensive to solve exactly. We

apply three domain-specific heuristics to reduce the search space and make it practically solvable.

First, we implement the remaining-workload histogram using fixed-size bins (e.g. 256 tokens), collapsing per-request variables into per-bin aggregates to reduce the optimization dimensionality. We use each bin’s upper bound as a conservative length estimate. The histogram predictor forecasts the per-bin request counts and achieves <9.8% relative error on our workload.

Second, we restrict the candidate configurations to a small, practical set. We prioritize intra-node TP and consider cross-node TP only in whole-node increments (e.g., 8 GPU’s). AFD candidates are also pre-selected via offline profiling to retain only a few high-performing Attention-to-FFN ratios.

Third, we adapt the candidate set within each generation step as the workload evolves. When the active batch is large and remaining lengths are moderate, we bias toward throughput-optimized modes. As the batch shrinks and long-tail sequences dominate, we prioritize latency-optimized modes to reduce tail completion time. For example, AFD can be effective with large batches by overlapping network communication with compute, but it often underperforms in the long tail scenario, where communication becomes difficult to hide and turns into the critical path.

4.2 Reactive Balancing

Proactive planning addresses structural shifts but struggles with transient imbalances caused by unpredictable output lengths and KV-cache pressure. To mitigate these transient stragglers, OrchestrRL uses a lightweight *Reactive Balancer* that periodically ranks workers by congestion and selectively migrates requests.

Without an oracle for each request’s response length, we define a congestion score LoadIndex_w (higher means more congested) for each Gen worker that combines queue pressure, KV headroom, and observed decoding rate:

$$\text{LoadIndex}_w = \frac{|Q_w^{\text{run}}| + |Q_w^{\text{wait}}|}{B^{\text{cap}}(M_w^{\text{free}})} \times \frac{1}{\tilde{R}_w}. \quad (5)$$

Here, $|Q_w^{\text{run}}|$ and $|Q_w^{\text{wait}}|$ denote the numbers of running and waiting requests. $B^{\text{cap}}(M_w^{\text{free}})$ represents the maximum concurrency allowed by the runtime KV allocator based on the current memory margin (M_w^{free}). \tilde{R}_w is the decoding throughput (tokens/s).

This design is driven by three insights: (1) *Queue depth is only meaningful relative to KV-limited concurrency*. Because generation lengths vary across requests, the same queue depth can indicate very different congestion under different KV headroom; we therefore normalize it by $B^{\text{cap}}(M_w^{\text{free}})$. (2) *Service rate matters*. Even with similar normalized backlogs,

	Ops	Profile			Fabrics	
		Volume	Frequency	Primitives	Possible Domain	Reconfigurability
Train. Stage	DP	High	Low	AllReduce	ToR-Agg-Core	High
	TP	Medium	High	AllReduce	HBD/ToR	Medium
	PP	Low	Low	P2P	ToR-Agg	High
	CP	Medium	High	P2P/All-to-All	ToR-Agg	Medium
	EP	Medium	High	All-to-All	ToR-Agg	Medium
Inter-Stage	WS	High	Low	T2G	ToR-Agg-Core	High
	RS	Low	Medium	G2T	ToR-Agg-Core	High
Gen. Stage	TP	Medium	High	AllReduce	HBD	Low
	EP	Medium	High	All-to-All	ToR-Agg	Low
	AFD	Low	High	M2N (Bipartite)	ToR-Agg	Low

Table 1: Communication profiles of the disaggregated RL workflow on a Clos-style fabric. For each operation, we summarize its dominant pattern (volume, frequency, primitives), which determines its placement scope (Possible Domain) and potential benefit from OCS reconfiguration over the EPS substrate (Reconfigurability). WS denotes weight synchronization and RS denotes response streaming; T2G and G2T denote Train to Gen and Gen to Train transfers.

workers with different decoding rates can have very different completion times; we include $1/\tilde{R}_w$. (3) *Migrations must be KV-feasible*. A migration is beneficial only if the destination can accommodate the request’s KV footprint without reducing the destination worker’s stable concurrency (i.e., effective batch size); LoadIndex ranks candidates, while KV-cache constraints gate feasibility.

To avoid thrashing, we migrate conservatively. Every interval, we compute $\Delta = \max_w \text{LoadIndex}_w - \min_w \text{LoadIndex}_w$ and trigger migration only if $\Delta > \theta$. We move requests from the most congested worker to the least congested, prioritizing the waiting queue under a short-context-first policy. A migration is performed only if the destination has sufficient KV headroom to host the request without reducing its stable batch size. The procedure stops once $\Delta \leq \theta$ or no further requests are feasible under KV constraints.

5 Dynamic Network Orchestration

Disaggregated RL creates stage-dependent time-varying communication that requires an adaptive network topology as established in §2.2. Our adaptive compute orchestration (§4) further incurs dynamic traffic. OrchestrRL complements compute scheduling with an adaptive fabric (RFabric) that provides (i) stage-aware topology reconfiguration and (ii) slack-aware orchestration that schedules circuit reconfiguration within each stage’s tolerance.

5.1 Overview

We adopt a hybrid EPS–OCS fabric called RFabric as depicted in Figure 7. For each stable communication period (within an RL stage), OrchestrRL selects a stage-aware topology template (§5.2) and proactively materializes the required OCS circuits in the aggregation/core layers, while the underlying host-facing packet-switched substrate remains unchanged.

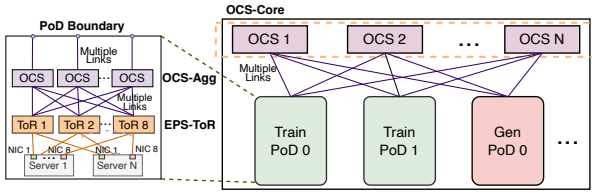


Figure 7: RFabric overview. Packet switching is performed at ToRs for host-facing connectivity and intra-ToR traffic. Above the ToR layer, aggregation and core connectivity are provided by reconfigurable OCS circuits.

Reconfiguration timing is governed by *safe windows* that can fully overlap the update cost; we detail this proactive orchestration in §5.3.

RFabric enforces a clear division of labor:

- **Access layer: Static EPS-ToR (rail-aligned).** As shown in Figure 7, servers connect exclusively to static EPS ToRs. We employ a rail-aligned strategy [1] here with compatibility for standard fat-trees. This electrical termination preserves stable host-facing links with low latency.
- **Aggregation & core layers: Dynamic OCS.** Above the ToR, RFabric uses reconfigurable OCS:
 - **OCS-Agg (intra-PoD):** Aggregation-layer OCS devices interconnect ToRs within a PoD, providing on-demand bandwidth for intra-PoD collectives (e.g., EP all-to-all) without changing any host-facing links.
 - **OCS-Core (inter-PoD):** Core-layer OCS devices interconnect PoDs, materializing inter-PoD paths only when needed.

Operationally, OrchestrRL steers traffic by scope. Traffic within a ToR uses the always-on EPS fabric. Traffic that spans ToRs (within a PoD) or PoDs is routed over the optical circuits accordingly. By reshaping only the upper-layer topology, OrchestrRL provides on-demand bandwidth without provisioning a worst-case static electrical core.

5.2 Stage-Aware Topology Reconfiguration

OrchestrRL operates RFabric via *dynamic topology materialization*: it re-configures optical circuits on-demand to instantiate a topology tailored to each stable communication period within an RL stage. We now describe (i) reconfiguration granularity across stages and (ii) the topology templates used for Train, Gen, and weight synchronization.

Reconfiguration granularity across RL stages. OrchestrRL adapts its reconfiguration frequency based on available slack across RL stages.

During Train, non-communication segments are often longer (e.g., due to large-batch execution), providing larger overlap opportunities. As a result, OrchestrRL can occasionally reconfigure within an iteration at selected stage-internal collective-free boundaries where the dominant primitive

or the participant set changes (e.g., attention-dominated vs. FFN/MoE), and at the transition from computation to gradient synchronization. During Gen, overlap is limited, so OrchestrRL uses coarse-grained reconfiguration. It typically keeps one circuit plan for each interval between deployment boundaries (parallelism/layout changes), selecting a template from the interval’s aggregated demand, provisioning OCS-Agg accordingly, and holding the plan until the next boundary. Finally, Weight Sync often provides ample non-critical slack, enabling on-demand reconfiguration right before the broadcast without extending the critical path.

Stage-specific topology templates. Figure 8 illustrates how OrchestrRL materializes distinct topologies to match the spatial heterogeneity characterized in §2, using the requirements summarized in Table 1.

1) High-bisection fabric for Train. Most Train traffic during forward/backward is intra-PoD. Accordingly, RFabric uses OCS-Agg to increase ToR-to-ToR bisection within a PoD (Figure 8(a)), sustaining layer-wise collectives such as All-to-All across servers. For DP AllReduce (gradient synchronization), which could span the whole Train clusters domain (Table 1), OrchestrRL additionally configures OCS-Core circuits to form a high-bisection inter-PoD mesh (Figure 8(b)). Although gradient exchange can be heavy for large models, it typically has limited overlap with other Train collectives, allowing these circuits to be time-shared efficiently.

2) Isolated intra-PoD fabrics for Gen. While Gen can be dominated by intra-server computation/communication (e.g., TP within a node), the *network-critical* portion is primarily localized cross-server traffic within each PoD (e.g., EP All-to-All [39] and M2N under AFD [62, 69]). As summarized in Table 1, this traffic largely resides in the ToR-Agg domain. Accordingly, RFabric leverages OCS-Agg to carve out independent intra-PoD topologies (Figure 8(c)), isolating Gen PoDs from each other and avoiding over-provisioning the core for traffic that rarely leaves a PoD. In our example, we reserve only a small slice of core bandwidth to connect Gen PoDs to the core, which is sufficient to stream generated responses back to Train PoDs.

3) Tree-style broadcast for weight synchronization. To accelerate periodic weight synchronization—an infrequent but high-volume transfer spanning many servers (Table 1)—RFabric materializes a temporary, circuit-scheduled dissemination *forest* using OCS-Core and OCS-Agg (Figure 8(d-e)), where each weight shard is disseminated via its own tree. The design is *two-level*. In Phase A, OCS-Core provisions inter-PoD point-to-point circuits from shard holders in Train PoDs to a small set of seed receivers in each destination Gen PoD, which serve as ingress points and fanout roots within the PoD. Each inter-PoD transfer also uses intra-PoD connectivity at both ends to reach boundary-facing uplinks

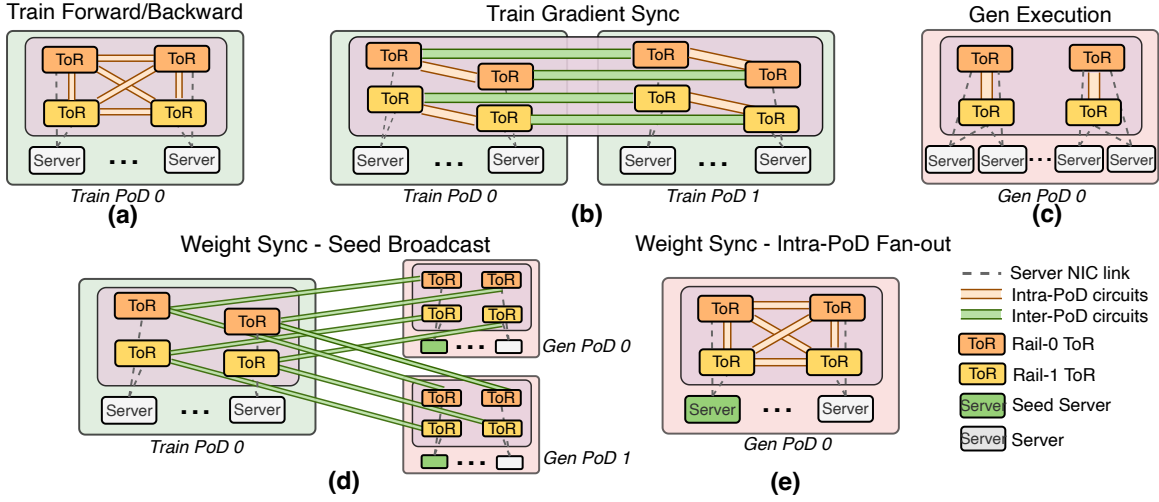


Figure 8: Dynamic topology materialization with RFabric across execution periods in different RL stages. Each PoD contains multiple servers; for clarity, each server is dual-homed with two NICs connected to rail-0 and rail-1 ToRs. Colored links denote OCS optical circuits (intra-PoD and inter-PoD, as indicated in the legend). During Train forward/backward, the fabric may reconfigure across model layers as the dominant communication pattern changes; we show a representative snapshot.

(via OCS-Agg and rack-local EPS). Phase A executes in multiple waves under a greedy, budget-aware scheduler that respects per-PoD boundary concurrency budgets (i.e., a cap on simultaneously active boundary-facing circuits incident to each PoD), preventing boundary-port hotspots. In Phase B, within each destination PoD, RFabric uses OCS-Agg (or rack-local EPS) to provision intra-PoD fanout from seeds to all remaining Gen ranks, avoiding redundant replication across the PoD boundary and alleviating root-NIC/ToR bottlenecks. Appendix E details the overlay construction and scheduling.

5.3 Orchestration for Proactive Reconfiguration

The runtime triggers reconfiguration only when the next *safe window*—a collective-free slack interval identified at runtime—is expected to cover the OCS update overhead at the chosen granularity; otherwise, OrchestrRL retains the current plan for that period. Building on the stage-aware templates (§5.2), OrchestrRL programs OCS devices via a dedicated control proxy running on an out-of-band control server/network. The proxy applies updates only within safe windows, using explicit runtime signals from lightweight instrumentation of collective boundaries. For each upcoming communication period, the runtime supplies an *intent* descriptor (stage type, dominant primitive mix, and group membership) and the expected transfer volume; the proxy materializes and commits the corresponding circuit plan in the next safe window (Algorithm 2).

The proxy operates in two phases:

Phase 1: Caching templates and allocation procedures.

In the first iteration of an RL job, the proxy identifies recurring communication periods at the per-stage reconfiguration granularity. For each period, it stores the intent descriptor and caches (i) the selected topology template and (ii) a demand-driven allocation procedure (Appendix D). At runtime, the cached procedure instantiates a concrete circuit plan from the current demand and fabric state (e.g., free ports and masked failures).

Phase 2: Proactive reconfiguration with runtime adaptation.

In subsequent iterations, given the cached template/procedure and runtime-announced participants/volumes, the proxy materializes a concrete circuit plan for the upcoming period. Using a ToR-centric view, it constructs demand at two scopes: (i) ToR-level demands within each PoD for ToR–ToR (intra-PoD) and ToR–uplink (inter-PoD lift/drop) circuits and (ii) a PoD-to-PoD summary to size OCS–Core inter-PoD capacity. The proxy then runs a greedy allocator (Appendix D) that iteratively adds one full-duplex circuit to the eligible pair with the largest *demand-to-capacity ratio* (i.e., demand divided by currently allocated circuit capacity), subject to port availability, until no demanded pair has free ports at both ends. Before committing, it performs a final end-to-end feasibility check (e.g., Core–Agg coupling and any state changes since materialization); if the check fails, it keeps the previous plan and retries in a later safe window.

5.4 Practical Considerations

Non-blocking reconfiguration. During topology reconfiguration, RFabric maintains switch-to-switch connectivity while dynamically adjusting the number of active links to

Algorithm 2 Topology Materialization

```

1: Input: demand  $D$  (for the upcoming communication period), intent  $I$ 
   (stage type / primitive mix / group membership), fabric state  $S$  (free
   ports, masked failures, link bandwidth  $B_{\text{link}}$ , previous plan  $C_{\text{prev}}$ )
2: Output: active circuit plan  $C_{\text{act}}$ 
3:  $tpl \leftarrow \text{GetCachedTemplate}(I)$   $\triangleright$  Populate on first iteration if missing
4:  $G \leftarrow \text{AggregateDemand}(D, I)$   $\triangleright$  PoD-level (core) and/or ToR-level
   (agg)
5:  $C \leftarrow \text{AllocateCircuits}(tpl, G, S)$   $\triangleright$  See Appendix D
6: if  $\neg \text{Validate}(C, S)$  then
7:   return  $C_{\text{prev}}$   $\triangleright$  Keep the last plan
8: COMMITINNEXTSAFEWINDOW}(C)
9: return  $C$ 
  
```

modulate bandwidth. Even if the topology materialization latency exceeds the required reconfiguration window, communication operations can proceed without stalling for the reconfiguration completion. Moreover, with the assistance of ECMP and re-routing, the available bandwidth for communication changes smoothly, at the cost of only a limited number of packet drops and reorders. Consequently, jobs can proceed with reduced, though not optimal, bandwidth until all switched links are fully activated.

Failure handling. RFabric is robust to device and link failures. Optical switching does not introduce new qualitative data-plane failure modes; it mainly changes which circuits are provisioned and the available bandwidth. RFabric terminates OCS at the ToR/aggregation layers, keeping host-facing EPS-ToR links always on and avoiding endpoint NIC/transceiver re-activation overheads seen with NIC-terminated OCS [46]. It handles failures at three layers: (i) *Server failures*: upon a GPU server failure, the job replaces failed ranks, and RFabric re-materializes optical connectivity to match the updated placement. (ii) *OCS failures*: if an OCS port/circuit is unavailable, the proxy masks the failed resources and reallocates circuits under the remaining port budget, typically reducing bandwidth but preserving connectivity. (iii) *EPS/NIC failures*: if an EPS link attached to a NIC fails, traffic can be relayed over the intra-server scale-up fabric (e.g., NVLink) to a healthy NIC and exit via its EPS links. We evaluate their performance impact in Appendix H.

6 Testbed Evaluation

Setup. We conducted experiments on an H800 testbed with servers interconnected by an 8×200Gbps RDMA network with a rail-optimized topology to validate the effectiveness of OrchestrRL’s compute scheduler. Adapted from veRL [57], we use Megatron-LM [58] as the training framework and a vLLM-based [44] backend for generation.

Baselines. We compare OrchestrRL against the following baselines of one-step asynchronous RL:

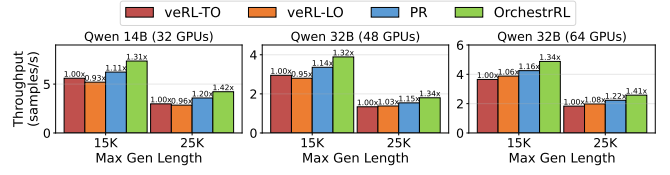


Figure 9: End-to-end throughput comparison across different schemes.

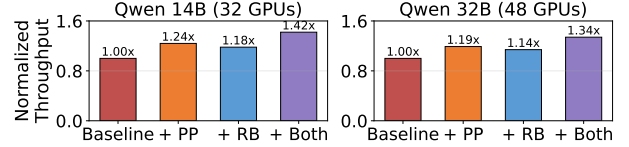


Figure 10: Improvement breakdown of OrchestrRL.

- **veRL-TO.** This baseline prioritizes DP to maximize the number of concurrent generation instances, tuning the DP-TP combination through a parameter sweep (TP = 1, 2, 4, 8) to achieve the best overall performance.
- **veRL-LO.** This baseline maximizes TP=8 for each generation instance to minimize latency.
- **Partial-rollout (PR).** An extension of veRL-TO, this approach enables partial rollouts, allowing a single response to be processed across two consecutive model versions. In this mode, a response can be truncated at one step and resumed in a subsequent step, though this may introduce greater staleness.

Workloads. We evaluate the Qwen-2.5 14B and 32B models [53] on the openr1-math-220k [7] and deepmath-103k [41] datasets, respectively, using the GRPO algorithm [55]. Model-related details are provided in Table 3 of Appendix C.

6.1 End-to-End Performance

Figure 9 reports the end-to-end throughput, defined as the average number of samples processed per second. OrchestrRL consistently outperforms all baselines. For Qwen-14B on 32 GPUs and Qwen-32B on 48 GPUs, we provision the training and generation clusters with the same number of GPUs. On 32 GPUs, OrchestrRL improves throughput over veRL-TO by 1.31× at a maximum generation length of 15K tokens and 1.42× at 25K tokens. On 48 GPUs with Qwen-32B, OrchestrRL achieves similar gains of 1.32× at 15K tokens and 1.34× at 25K tokens. We observe the same trend for Qwen-32B on 64 GPUs (with 40 GPUs allocated to generation). Overall, these results highlight the benefit of OrchestrRL’s adaptive compute scheduling, consistent with the case study in §6.2.2.

6.2 Ablations and Analysis

6.2.1 Ablation study. Proactive planning (+PP) adapts parallelism within a generation step to the evolving workload,

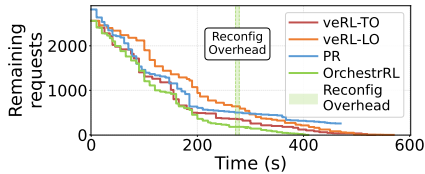


Figure 11: Remaining requests in a generation step across different schemes.

improving throughput to $1.24\times$ on Qwen-14B and $1.19\times$ on Qwen-32B over veRL-TO (Figure 10). Reactive balancing (+RB) is also beneficial ($1.18\times/1.14\times$), using lightweight on-the-fly request migrations to mitigate output-length variability and KV-cache imbalance. Combining the two delivers the largest gains, reaching $1.42\times$ and $1.34\times$.

6.2.2 Case study. We present remaining-request curves for Qwen-14B in Figure 11. veRL-LO starts with low concurrency (a few TP=8 instances), limiting early parallelism and slowing progress. veRL-TO uses eight TP=2 instances, clearing the initial batch quickly but becoming less efficient as concurrency drops; it still finishes faster than veRL-LO. PR starts with more remaining requests due to truncation from the previous step and ends with truncation under its rollout policy. OrchestrRL adapts to the workload by balancing requests and reconfiguring parallelism, switching from eight TP=2 to two TP=8 instances to shorten the tail. Although reconfiguration adds ~ 7.5 s overhead (mainly 1.5s for switching and 5.4s for KV-cache recomputation) at around 272s, OrchestrRL achieves the shortest completion time. Optimization solving time is negligible in this setting; detailed results are shown in Figure 20 (Appendix F).

7 Large-Scale Simulation

To evaluate RFabric and the large-scale behavior of OrchestrRL, we build RLSim, a high-fidelity simulator for disaggregated RL at cluster scale. RLSim integrates (i) a training simulator, (ii) an inference simulator based on Frontier [34], and (iii) a packet-level network simulator extended from htsim [5]. These components model the end-to-end RL pipeline, support multiple network topologies, and capture diverse collective communication patterns.

We use RLSim to (1) validate fidelity by matching per-stage training, inference, and network behaviors against measurements, (2) evaluate RFabric’s performance-cost trade-offs against alternative fabrics, and (3) co-simulate OrchestrRL by integrating its compute scheduler with RFabric, reporting end-to-end throughput and throughput per dollar. We primarily evaluate a dense Qwen-2.5-72B model [53] and the Qwen2-57B-A14B MoE model [8]. We use input- and output-length traces collected on our testbed with deepmath-103k [41] and scale them to match the simulated GPU count. Detailed model configurations are provided in Appendix C.

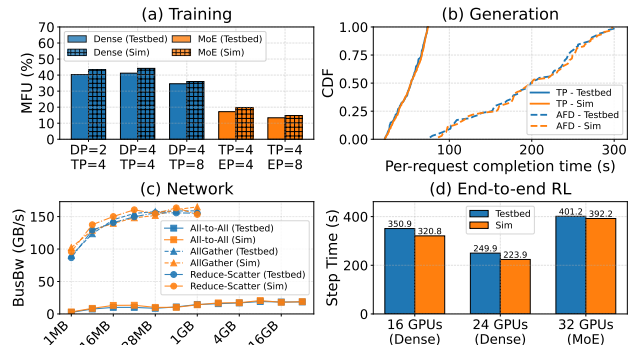


Figure 12: RLSim fidelity evaluation. In (c), the all-gather data size refers to the input tensor size, while the reduce-scatter data size refers to the output tensor size.

7.1 Simulator Fidelity

Here, we evaluate the fidelity of RLSim by validating its key components as well as the end-to-end workflow.

Training. We evaluate fidelity by comparing model FLOP utilization (MFU) under a fixed workload (global batch size 512, sequence length 5120). We sweep DP/TP/EP for dense and MoE training on 8–32 GPUs (Figure 12(a)). RLSim closely matches the testbed MFU levels and trends, with at most 8.86% error.

Generation. We assess RLSim’s inference fidelity with batch size 256, prompt length 512, and generation lengths from 1024 to 4096. Figure 12(b) plots the completion time CDFs, showing that RLSim closely tracks the testbed result: the mean error is 3.3% for TP and 5.95% for AFD.¹

Network. We validate the packet-level network simulator by calibrating it to our rail-optimized fabric and replaying NCCL-style collective microbenchmarks across message sizes. We compare bus bandwidth on a 5-server (40-GPU) testbed against RLSim (Figure 12(c)). RLSim matches the testbed within 5.98% average error.

End-to-end RL. Finally, we validate end-to-end fidelity by measuring per-step wall-clock time of a full RL iteration (Figure 12(d)). Across different configurations for dense and MoE models, RLSim achieves errors of 2.2% to 10.4%.

7.2 Network-Centric Results

Setup. Unless otherwise specified, we set the per-link propagation latency to $1\ \mu\text{s}$ and the per-hop switch processing latency to $0.8\ \mu\text{s}$, following [46]. We use an MTU of 9216 B and simulate packet-level queuing and congestion with identical NIC, link, and switch parameters across all evaluated topologies to ensure a fair comparison. Each server hosts eight NVIDIA H800 GPUs and eight NICs (one per GPU); each NIC provides bandwidth B (default 200 Gbps). Intra-server

¹Due to the lack of publicly available AFD implementation, we are only able to use an internal codebase with an internal MoE model for calibration.

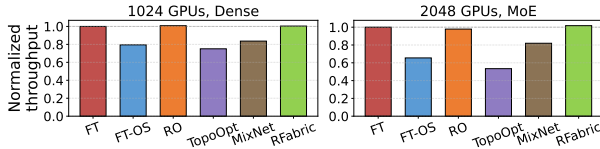


Figure 13: End-to-end performance comparison across different scales.

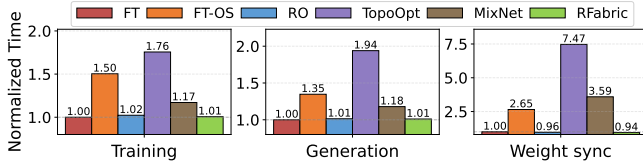


Figure 14: Stage-wise performance under different network fabrics for Qwen-57B-MoE model.

GPUs are connected via NVLink, providing an effective bidirectional bandwidth of 400 GB/s per GPU. For OCS-based designs, we model topology-dependent circuit connectivity and routing, assuming a 25 ms reconfiguration overhead unless specified otherwise. With a given budget, we allocate the number of GPUs to Train and Gen following [67].

Baselines. We compare the performance of RFabric with the following interconnects:

- **Fat-tree (FT)** [29]. A non-blocking Fat-tree network.
- **OverSub. Fat-tree (FT-OS)**. A Fat-tree interconnect with the 3:1 over-subscription ratio.
- **Rail-optimized (RO)**. A non-blocking Fat-tree variant that connects same-rank GPUs to the same ToR switch, reducing intra-rail latency [1].
- **TopoOpt** [63]. An optical interconnect that all NICs are optimistically connected directly via optical patch panels, which share a similar topology with [43].
- **MixNet** [46]. A state-of-the-art hybrid EPS-OCS fabric: in each 8-GPU server, 6 GPUs connect to a local OCS, while 2 provide scale-out connectivity via a non-blocking Fat-tree.

7.2.1 End-to-end performance. Figure 13 illustrates significant throughput losses for FT-OS and TopoOpt. FT-OS is constrained by oversubscription, while TopoOpt struggles to provide sufficient scale-out bandwidth for Train-time gradient synchronization and Train/Gen weight synchronization. Its performance further degrades for bandwidth-sensitive collectives (e.g., all-to-all) when host-level forwarding is required, achieving only 0.47–0.76× of FT, with worse results on MoE models. Similarly, MixNet underperforms due to limited scale-out connectivity for DP traffic and large-scale weight synchronization, reaching approximately 0.81× of FT. In contrast, RFabric remains close to FT and RO, leveraging its flexible hybrid topology and stage-aware reconfiguration across RL stages.

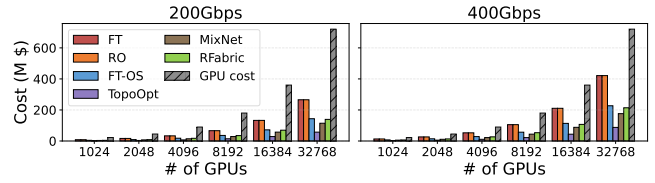


Figure 15: Network cost comparison at 200Gbps and 400Gbps. GPU cost is shown as reference. Detailed pricing is provided in Appendix G.

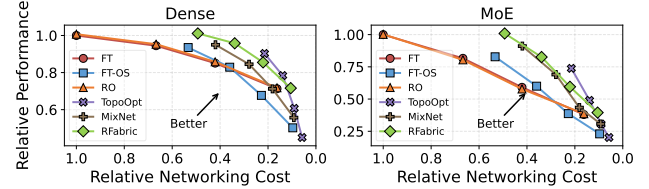


Figure 16: Performance-cost trade-off under different interconnect link speeds. For each curve, the four markers from left to right correspond to 800/400/200/100 Gbps.

7.2.2 Stage-wise performance breakdown. Figure 14 reports the per-stage time of Qwen2.5-57B-MoE across Train, Gen (AFD mode), and Weight Sync, normalized to FT. RFabric stays close to FT across all stages, matching RO and yielding a small improvement in Weight Sync by leveraging optical circuits for bulk transfers. In contrast, FT-OS, TopoOpt, and MixNet are consistently slower to varying degrees.

7.2.3 Network cost. We analyze network costs for clusters with 200Gbps and 400Gbps links (Figure 15). The FT is the high-cost baseline (1.00×), and Rail-Optimized has similar cost. Oversubscribed FT reduces cost to 0.54×, while TopoOpt further lowers it to 0.21× at the expense of reduced scale-out bandwidth for global collectives. In contrast, RFabric costs 0.51–0.52× of FT, comparable to MixNet and FT-OS; this relative ordering is consistent across link speeds. Importantly, although GPU cost remains higher than network cost in absolute terms, faster links increase the network-to-GPU cost ratio: for FT, network cost grows from ~37% of GPU cost at 200Gbps to ~59% at 400Gbps, making network cost control increasingly important at higher link rates.

7.2.4 Performance-cost pareto frontier. Figure 16 summarizes the performance-cost trade-off under four link speeds. RFabric stays on or near the Pareto frontier, providing higher performance at a given cost (or lower cost at a given performance) than most alternatives. In particular, TopoOpt and FT-OS reduce cost but suffer substantial performance degradation, placing them well below the frontier. Compared with high-performance baselines, RFabric improves cost-efficiency by 1.53×–2.06× over FT and by 1.61×–2.08× over RO, and by ~1.13× over MixNet.

7.2.5 OCS-related sensitivity analysis. We evaluate sensitivity to (i) OCS reconfiguration delay T_{ocs} and (ii) the

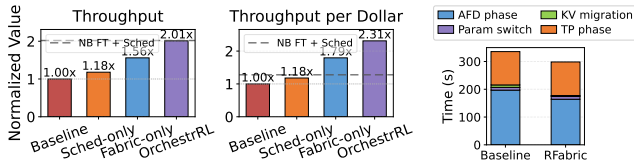


Figure 17: Co-design comparison. Figure 18: Network Dashed line is a reference setup of full impact on compute Fat-tree and OrchestrRL’s compute scheduler in Gen. scheduler.

circuit allocation policy (Appendix I). As discussed in §5, T_{ocs} impacts stages differently: Train can tolerate tens of milliseconds due to slack; Gen cannot reconfigure on the critical path and thus only reconfigures at coarse deployment boundaries; and Weight Sync is largely insensitive over practical ranges given its ample slack. We also compare traffic-aware allocation with uniform splitting, finding the former superior as it focuses circuits on bottleneck pairs, while the latter wastes capacity on low-demand links.

7.3 Co-Simulation

Setup. We evaluate the compute-network co-design in OrchestrRL through a 2×2 factorial ablation study, considering two key factors: (i) compute scheduling (OrchestrRL scheduler vs. a fixed baseline) and (ii) network fabric (RFabric vs. a cost-comparable static Fat-tree network with 3:1 oversubscription). This results in four configurations: *Baseline*, *Sched-only*, *Fabric-only*, and *OrchestrRL*. We evaluate Qwen3-235B-A22B [9] on 2048 GPUs.

7.3.1 End-to-end results. Figure 17 reports end-to-end throughput and throughput-per-dollar (TPD), both normalized to the baseline, where $TPD = \text{Throughput}/\text{Cost}$, with *Cost* including total network cost.

Throughput. As shown in Figure 17(a), *Sched-only* achieves a modest 1.18 \times throughput gain, while *Fabric-only* improves throughput to 1.56 \times , underscoring the network bottleneck under the oversubscribed Fat-tree baseline. Combining both, OrchestrRL achieves the highest throughput (2.01 \times), matching the non-blocking Fat-tree + scheduler reference.

Cost efficiency. Figure 17(b) shows *Sched-only* improves TPD by 1.18 \times , while *Fabric-only* achieves 1.79 \times by improving performance and reducing costs. OrchestrRL combines both benefits, delivering the best TPD (2.31 \times) and outperforming the non-blocking Fat-tree + scheduler reference, which incurs significantly higher network cost.

7.3.2 Network’s impact on compute reconfiguration. To quantify how the fabric interacts with OrchestrRL’s compute scheduler during reconfiguration, we compare a representative Gen step on RFabric to a cost-comparable oversubscribed Fat-tree. The step transitions from 35 AFD instances (each using 3×8 GPUs for attention and 2×8 GPUs for MoE)

to 175 TP= 8 instances, triggering model-parameter reloads and KV-cache migration across servers. With RFabric, the AFD phase time drops by 16.7% and KV-cache migration by 58.3%, while parameter switching and the TP phase remain essentially unchanged. Overall, RFabric reduces end-to-end Gen step time by 10.7% versus the baseline.

8 Related Work

RL training frameworks. Many frameworks accelerate RL training, spanning co-located designs and their optimizations [42, 57, 68] as well as newer asynchronous, disaggregated systems such as StreamRL and Laminar [35, 42, 56, 57, 67]. OrchestrRL targets one-step asynchrony to balance stability and throughput, focusing on the generation bottleneck and a co-designed network fabric.

Generation optimization in RL. Generation is a key bottleneck in RL due to the long-tailed distribution of output lengths [36, 56, 64, 65, 67]. Prior methods address this with speculative decoding [40, 52] and partial rollouts [35, 36], mostly in synchronous settings, though some [35, 36] incur additional staleness. OrchestrRL expands the design space by dynamically adapting parallelism and performing lightweight, on-the-fly load balancing, mitigating stragglers caused by variable output lengths and uneven KV-cache usage—without introducing extra staleness. Agentic RL with external tools needs to optimize per-request workflows [45, 60]; OrchestrRL is complementary and can integrate into such pipelines, primarily targeting RL reasoning settings

OCS-related network architectures. Prior hybrid packet/circuit DCNs primarily optimize for general traffic patterns, failing to capture the phase-varying collective communication in modern LLM/RL workloads. This often results in connectivity mismatches or reconfiguration misaligned with stage-level communication periods [30, 33, 37, 38, 49, 51, 59, 61]. Recent approaches [32, 43, 63], such as SiP-ML [43] and TopoOpt [63], co-optimize topology and parallelization but rely on centralized, one-shot OCS reconfiguration, limiting their ability to support large-scale heterogeneous parallelism (e.g., MoE). While MixNet [46] introduces regional reconfigurability for MoE training, it confines reconfiguration to local domains with GPU-terminated circuits, restricting cluster-wide bandwidth and flexibility for latency-sensitive tasks. In contrast, RFabric is the first OCS-based fabric designed explicitly for disaggregated RL. It enables phase-aware, multi-granularity reconfiguration across training, generation, and weight synchronization using higher-tier OCS connectivity, addressing the limitations of prior systems.

9 Conclusion

This paper presents OrchestrRL, an orchestration framework for disaggregated RL that mitigates inefficiencies caused by workload dynamics. OrchestrRL includes a compute scheduler that switches parallelism and balances requests during generation to reduce makespan. It also integrates RFabric, a reconfigurable EPS-OCS fabric that adapts topology to demand, avoiding network overprovisioning while sustaining performance. Our evaluation shows substantial gains in throughput and cost efficiency.

References

- [1] Doubling all2all performance with nvidia collective communication library 2.12. <https://developer.nvidia.com/blog/doubling-all2all-performance-with-nvidia-collective-communication-library-2-12-2022>.
- [2] Coherent announces optical circuit switch for data centers based on ultrareliable dlx technology. <https://www.coherent.com/news/press-releases/optical-circuit-switch-for-data-centers-live-demo-at-ofc-2024-based-on-ultrareliable-dlx-technology>, 2024.
- [3] Claude-4. <https://www.anthropic.com/news/claude-4>, 2025.
- [4] Gpt-5. <https://openai.com/index/gpt-5-new-era-of-work/>, 2025.
- [5] htsim. <https://github.com/Broadcom/csg-htsim/>, 2025.
- [6] Megatron-LM. <https://github.com/NVIDIA/Megatron-LM/tree/main/>, 2025.
- [7] OpenR1-Math-220k. <https://huggingface.co/datasets/openr1/OpenR1-Math-220k/>, 2025.
- [8] Qwen2-57B-A14B. <https://huggingface.co/Qwen/Qwen2-57B-A14B/tree/main/>, 2025.
- [9] Qwen3-235B-A22B. <https://huggingface.co/Qwen/Qwen3-235B-A22B/tree/main/>, 2025.
- [10] Zero-Reload Model Switching with vLLM Sleep Mode. <https://blog.vllm.ai/2025/10/26/sleep-mode.html>, 2025.
- [11] 400GBASE-DR4 QSFP-DD PAM4 Silicon Photonics Transceiver. <https://www.fs.com/products/173589.html>, 2026.
- [12] 800G OSFP 2xDR4/DR8 PAM4 Transceiver. <https://www.fs.com/c/800g-osfp-qsf-dd-4089>, 2026.
- [13] Arista 7060X6-64PE 64PE-B-64x 800GbE. <https://www.grabnpay.in/products/arista-7060x6-64pe-b-64-800gbe-osfp-2-sfp-leaf-spine-data-centre-switch-1ru?variant=50080426819888>, 2026.
- [14] C2G 1m LC-LC Duplex Single Mode OS2 Fiber Cable. <https://www.dell.com/en-us/shop/c2g-1m-lc-lc-9-125-duplex-single-mode-os2-fiber-cable/apd/a7104249>, 2026.
- [15] Calient's Optical Circuit Switch (OCS) - S320. <https://signalsolutions.eu/product/optical-circuit-switches-calient/>, 2026.
- [16] Cisco Nexus 9300 (64x 400G). <https://www.zones.com/site/product/index.html?id=110646707>, 2026.
- [17] Cisco QSFP-100G-CWDM4-S Compatible 100GBASE-CWDM4 QSFP28 Transceiver. <https://www.fs.com/products/65214.html>, 2026.
- [18] Cisco QSFP-200G-SR4-S Compatible 200GBase SR4 QSFP56 MMF Transceiver. <https://proficium.com/collections/200g-qsf56-sr4-optical-transceivers>, 2026.
- [19] Edgecore AS7816-64X 64-Port 100GbE QSFP28 Switch Pricing. <https://www.ebay.com/itm/357652027117>, 2026.
- [20] MPO-12 Trunk Cable Single Mode OS2. <https://www.compufox.com/12-Fiber-MTP-MPO-Patch-Cables-s/3206.html>, 2026.
- [21] MPO12 to MPO12 Single-Mode OS2 Fiber Jumper. <https://fluxlight.com/FL-MPO12-MPO12-OS2-5M/>, 2026.
- [22] NVIDIA ConnectX-6 Dx MCX623106AN-CDAT 200GbE SmartNIC. https://www.naddod.com/products/nvidia-networking/102174?srsId=AfmBOorP7tykh8jZAzPrFeMVMmF9xciZPZxi5R3T2D_3rksvy9_NBYj, 2026.
- [23] NVIDIA ConnectX-7 NDR 400G InfiniBand/Ethernet Adapter Card. <https://www.dell.com/en-us/shop/nvidia-connectx-7-ndr-400g-infiniband-adapter-card/apd/ac478006>, 2026.
- [24] NVIDIA ConnectX-8 C8180 HHHL SuperNIC, 800Gbps. <https://www.shi.com/product/50537403>, 2026.
- [25] NVIDIA Mellanox MCX516A-CCAT ConnectX-5 EN Network Interface Card. <https://www.fs.com/products/119647.html>, 2026.
- [26] NVIDIA SN4600 ETHERNET SWITCH WITH CUMULUS. 64 QSFP56 200G PORTS. <https://www.shi.com/product/49444542/NVIDIA-SN4600-ETHER>, 2026.
- [27] POLATIS Series 7000. <https://www.polatis.com/series-7000-384x384-port-software-controlled-optical-circuit-switch-sdn-enabled.asp>, 2026.
- [28] Single Mode OS2 MPO-16 to MPO-16 Trunk Cable, 16 Fiber, Female, Type B, LSZH. https://www.optcore.net/product/mt-mpo16-f-mpo16-f-16sm-xm-b-ls/?srsId=AfmBOoq_tsajd_vZHQev5ZuzjtPekkbvmow0OzWR0cR-nSVIILLtMr3, 2026.
- [29] Mohammad Al-Fares, Alexander Loukissas, and Amin Vahdat. A scalable, commodity data center network architecture. *ACM SIGCOMM computer communication review*, 2008.
- [30] Mohammad Al-Fares, Sivasankar Radhakrishnan, Barath Raghavan, Nelson Huang, and Amin Vahdat. Hedera: dynamic flow scheduling for data center networks. In *USENIX NSDI*, 2010.
- [31] George EP Box, Gwilym M Jenkins, Gregory C Reinsel, and Greta M Ljung. *Time series analysis: forecasting and control*. John Wiley & Sons, 2015.
- [32] Eric Ding, Chuhan Ouyang, and Rachee Singh. Photonic rails in ml datacenters. In *Proceedings of the 24th ACM Workshop on Hot Topics in Networks*, pages 149–159, 2025.
- [33] Nathan Farrington, George Porter, Sivasankar Radhakrishnan, Hamid Hajabdolali Bazzaz, Vikram Subramanya, Yeshaiah Fainman, George Papen, and Amin Vahdat. Helios: A hybrid electrical/optical switch architecture for modular data centers. In *SIGCOMM*, 2010.
- [34] Yicheng Feng, Xin Tan, Kin Hang Sew, Yimin Jiang, Yibo Zhu, and Hong Xu. Frontier: Simulating the next generation of llm inference systems. *arXiv preprint arXiv:2508.03148*, 2025.
- [35] Wei Fu, Jiaxuan Gao, Xujie Shen, Chen Zhu, Zhiyu Mei, Chuyi He, Shusheng Xu, Guo Wei, Jun Mei, Jiashu Wang, Tongkai Yang, Binhang Yuan, and Yi Wu. Areal: A large-scale asynchronous reinforcement learning system for language reasoning, 2025.
- [36] Wei Gao, Yuheng Zhao, Dakai An, Tianyuan Wu, Lunxi Cao, Shaopan Xiong, Ju Huang, Weixun Wang, Siran Yang, Wenbo Su, Jiamang Wang, Lin Qu, Bo Zheng, and Wei Wang. Rollpacker: Mitigating long-tail rollouts for fast, synchronous rl post-training. *arXiv preprint arXiv:2509.21009*, 2025.
- [37] Albert Greenberg, James R. Hamilton, Navendu Jain, Srikanth Kandula, Changhoon Kim, Parantap Lahiri, David A. Maltz, Parveen Patel, and Sudipta Sengupta. VL2: a scalable and flexible data center network. In *SIGCOMM Comput. Commun. Rev.*, 2009.
- [38] Chuanxiong Guo, Guohan Lu, Dan Li, Haitao Wu, Xuan Zhang, Yunfeng Shi, Chen Tian, Yongguang Zhang, and Songwu Lu. Bcube: a high performance, server-centric network architecture for modular data centers. In *SIGCOMM Comput. Commun. Rev.*, 2009.
- [39] Daya Guo, Dejian Yang, Haowei Zhang, Junxiao Song, Ruoyu Zhang, Runxin Xu, Qihao Zhu, Shirong Ma, Peiyi Wang, Xiao Bi, et al. Deepseek-r1: Incentivizing reasoning capability in llms via reinforcement learning. *arXiv preprint arXiv:2501.12948*, 2025.
- [40] Jingkai He, Tianjian Li, Erhu Feng, Dong Du, Qian Liu, Tao Liu, Yubin Xia, and Haibo Chen. History rhymes: Accelerating llm reinforcement learning with rhymelr. *arXiv preprint arXiv:2508.18588*, 2025.
- [41] Zhiwei He, Tian Liang, Jiahao Xu, Qiuzhi Liu, Xingyu Chen, Yue Wang, Linfeng Song, Dian Yu, Zhenwen Liang, Wenxuan Wang, et al. Deepmath-103k: A large-scale, challenging, decontaminated, and verifiable mathematical dataset for advancing reasoning. *arXiv preprint arXiv:2504.11456*, 2025.
- [42] Jian Hu, Xibin Wu, Zilin Zhu, Xianyu, Weixun Wang, Dehao Zhang, and Yu Cao. Openrlhf: An easy-to-use, scalable and high-performance rlhf framework. *arXiv preprint arXiv:2405.11143*, 2024.
- [43] Mehرداد Khani, Manya Ghobadi, Mohammad Alizadeh, Ziyi Zhu, Madeleine Glick, Keren Bergman, Amin Vahdat, Benjamin Klenk, and Eiman Ebrahimi. Sip-ml: high-bandwidth optical network interconnects for machine learning training. In *Proceedings of the 2021 ACM*

SIGCOMM 2021 Conference, 2021.

- [44] Woosuk Kwon, Zhuohan Li, Siyuan Zhuang, Ying Sheng, Lianmin Zheng, Cody Hao Yu, Joseph Gonzalez, Hao Zhang, and Ion Stoica. Efficient memory management for large language model serving with pagedattention. In *Proceedings of the 29th symposium on operating systems principles*, pages 611–626, 2023.
- [45] Hanchen Li, Qiuyang Mang, Runyuan He, Qizheng Zhang, Huanzhi Mao, Xiaokun Chen, Alvin Cheung, Joseph Gonzalez, and Ion Stoica. Continuum: Efficient and robust multi-turn llm agent scheduling with kv cache time-to-live. *arXiv preprint arXiv:2511.02230*, 2025.
- [46] Xudong Liao, Yijun Sun, Han Tian, Xinchun Wan, Yilun Jin, Zilong Wang, Zhenghang Ren, Xinyang Huang, Wenxue Li, Kin Fai Tse, Zhizhen Zhong, Guyue Liu, Ying Zhang, Xiaofeng Ye, Yiming Zhang, and Kai Chen. Mixnet: A runtime reconfigurable optical-electrical fabric for distributed mixture-of-experts training. In *Proceedings of the ACM SIGCOMM 2025 Conference*, 2025.
- [47] Diego Lugones, Konstantinos Christodoulopoulos, Kostas Katrinis, Marco Ruffini, Donal O’Mahony, and Martin Collier. Accelerating communication-intensive parallel workloads using commodity optical switches and a software-configurable control stack. In *Euro-Par 2013 Parallel Processing*, 2013.
- [48] William M Mellette, Rajdeep Das, Yibo Guo, Rob McGuinness, Alex C Snoeren, and George Porter. Expanding across time to deliver bandwidth efficiency and low latency. In *17th USENIX Symposium on Networked Systems Design and Implementation (NSDI 20)*, 2020.
- [49] Radhika Niranjan Mysore, Andreas Pamboris, Nathan Farrington, Nelson Huang, Pardis Miri, Sivasankar Radhakrishnan, Vikram Subramanya, and Amin Vahdat. Portland: a scalable fault-tolerant layer 2 data center network fabric. In *Proceedings of the ACM SIGCOMM 2009 Conference on Data Communication*, 2009.
- [50] Michael Noukhovitch, Shengyi Huang, Sophie Xhonneux, Arian Hoseini, Rishabh Agarwal, and Aaron Courville. Asynchronous rlhf: Faster and more efficient off-policy rl for language models. *arXiv preprint arXiv:2410.18252*, 2024.
- [51] Leon Poutievski, Omid Mashayekhi, Joon Ong, Arjun Singh, Mukarram Tariq, Rui Wang, Jianan Zhang, Virginia Beaugard, Patrick Conner, Steve Gribble, et al. Jupiter evolving: transforming google’s datacenter network via optical circuit switches and software-defined networking. In *Proceedings of the ACM SIGCOMM 2022 Conference*, pages 66–85, 2022.
- [52] Ruoyu Qin, Weiran He, Weixiao Huang, Yangkun Zhang, Yikai Zhao, Bo Pang, Xinran Xu, Yingdi Shan, Yongwei Wu, and Mingxing Zhang. Seer: Online context learning for fast synchronous llm reinforcement learning. *arXiv preprint arXiv:2511.14617*, 2025.
- [53] Qwen, :, An Yang, Baosong Yang, Beichen Zhang, Binyuan Hui, Bo Zheng, Bowen Yu, Chengyuan Li, Dayiheng Liu, Fei Huang, Haoran Wei, Huan Lin, Jian Yang, Jianhong Tu, Jianwei Zhang, Jianxin Yang, Jiayi Yang, Jingren Zhou, Junyang Lin, Kai Dang, Keming Lu, Keqin Bao, Kexin Yang, Le Yu, Mei Li, Mingfeng Xue, Pei Zhang, Qin Zhu, Rui Men, Runji Lin, Tianhao Li, Tianyi Tang, Tingyu Xia, Xingzhang Ren, Xuancheng Ren, Yang Fan, Yang Su, Yichang Zhang, Yu Wan, Yuqiong Liu, Zeyu Cui, Zhenru Zhang, and Zihan Qiu. Qwen2.5 technical report. *arXiv preprint arXiv:2412.15115*, 2025.
- [54] R Ryf, J Kim, JP Hickey, A Gnauck, D Carr, F Pardo, C Bolle, R Frahm, N Basavanthally, C Yoh, et al. 1296-port mems transparent optical crossconnect with 2.07 petabit/s switch capacity. In *OFC 2001. Optical Fiber Communication Conference and Exhibit. Technical Digest Postconference Edition (IEEE Cat. 01CH37171)*, volume 4, pages PD28–PD28. IEEE, 2001.
- [55] Zhihong Shao, Peiyi Wang, Qihao Zhu, Runxin Xu, Junxiao Song, Xiao Bi, Haowei Zhang, Mingchuan Zhang, YK Li, Yang Wu, et al. Deepseekmath: Pushing the limits of mathematical reasoning in open language models. *arXiv preprint arXiv:2402.03300*, 2024.
- [56] Guangming Sheng, Yuxuan Tong, Borui Wan, Wang Zhang, Chaobo Jia, Xibin Wu, Yuqi Wu, Xiang Li, Chi Zhang, Yanghua Peng, et al. Laminar: A scalable asynchronous rl post-training framework. *arXiv preprint arXiv:2510.12633*, 2025.
- [57] Guangming Sheng, Chi Zhang, Zilingfeng Ye, Xibin Wu, Wang Zhang, Ru Zhang, Yanghua Peng, Haibin Lin, and Chuan Wu. Hybridflow: A flexible and efficient rlhf framework. In *Proceedings of the Twentieth European Conference on Computer Systems*, pages 1279–1297, 2025.
- [58] Mohammad Shoeybi, Mostofa Patwary, Raul Puri, Patrick LeGresley, Jared Casper, and Bryan Catanzaro. Megatron-lm: Training multi-billion parameter language models using model parallelism. *arXiv preprint arXiv:1909.08053*, 2019.
- [59] Ankit Singla, Chi-Yao Hong, Lucian Popa, and P. Brighten Godfrey. Jellyfish: Networking data centers randomly. In *USENIX NSDI*, 2012.
- [60] Xin Tan, Yimin Jiang, Yitao Yang, and Hong Xu. Towards end-to-end optimization of llm-based applications with ayo. In *Proceedings of the 30th ACM International Conference on Architectural Support for Programming Languages and Operating Systems, Volume 2*, 2025.
- [61] Ryohei Urata, Hong Liu, Kevin Yasumura, Erji Mao, Jill Berger, Xiang Zhou, Cedric F. Lam, Roy Bannon, Darren Hutchinson, Dan Nelson, Leonid B. Poutievski, Arjun Singh, Joon Suan Ong, and Amin Vahdat. Mission apollo: Landing optical circuit switching at datacenter scale. *ArXiv*, abs/2208.10041, 2022.
- [62] Bin Wang, Bojun Wang, Changyi Wan, Guanzhe Huang, Hanpeng Hu, Haonan Jia, Hao Nie, Mingliang Li, Nuo Chen, Siyu Chen, et al. Step-3 is large yet affordable: Model-system co-design for cost-effective decoding. *arXiv preprint arXiv:2507.19427*, 2025.
- [63] Weiyang Wang, Moein Khazraee, Zhizhen Zhong, Manya Ghobadi, Zhihao Jia, Dheevatsa Mudigere, Ying Zhang, and Anthony Kewitsch. TopoOpt: Co-optimizing network topology and parallelization strategy for distributed training jobs. In *20th USENIX Symposium on Networked Systems Design and Implementation (NSDI 23)*, 2023.
- [64] Bo Wu, Sid Wang, Yunhao Tang, Jia Ding, Eryk Helenowski, Liang Tan, Tengyu Xu, Tushar Gowda, Zhengxing Chen, Chen Zhu, et al. Llamarl: A distributed asynchronous reinforcement learning framework for efficient large-scale llm training. *arXiv preprint arXiv:2505.24034*, 2025.
- [65] Long Zhao, Qinghe Wang, Jian Zhu, Youhui Bai, Zewen Jin, Chaoyi Ruan, Shengnan Wang, and Cheng Li. Accelerating generation in RLHF by phase-aware tensor parallelism. The 1st Frontier AI Systems Workshop, 2025.
- [66] Yinmin Zhong, Shengyu Liu, Junda Chen, Jianbo Hu, Yibo Zhu, Xuanzhe Liu, Xin Jin, and Hao Zhang. {DistServe}: Disaggregating prefill and decoding for goodput-optimized large language model serving. In *18th USENIX Symposium on Operating Systems Design and Implementation (OSDI 24)*, 2024.
- [67] Yinmin Zhong, Zili Zhang, Xiaoniu Song, Hanpeng Hu, Chao Jin, Bingyang Wu, Nuo Chen, Yukun Chen, Yu Zhou, Changyi Wan, et al. Streamrl: Scalable, heterogeneous, and elastic rl for llms with disaggregated stream generation. *arXiv preprint arXiv:2504.15930*, 2025.
- [68] Yinmin Zhong, Zili Zhang, Bingyang Wu, Shengyu Liu, Yukun Chen, Changyi Wan, Hanpeng Hu, Lei Xia, Ranchen Ming, Yibo Zhu, et al. Optimizing rlhf training for large language models with stage fusion. *arXiv preprint arXiv:2409.13221*, 2024.
- [69] Ruidong Zhu, Ziheng Jiang, Chao Jin, Peng Wu, Cesar A Stuardo, Dongyang Wang, Xinlei Zhang, Huaping Zhou, Haoran Wei, Yang Cheng, et al. Megascale-infer: Serving mixture-of-experts at scale with disaggregated expert parallelism. *arXiv preprint arXiv:2504.02263*, 2025.

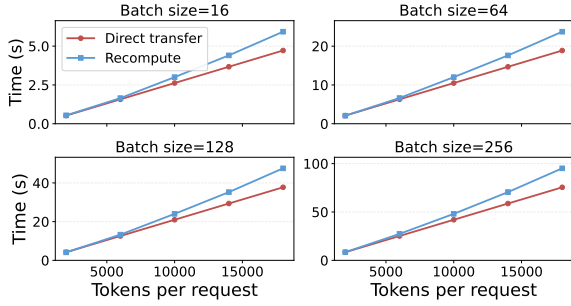


Figure 19: Time cost comparison between (i) direct KV cache transfer with one 200Gbps NIC and (ii) recomputation, across different batch sizes and generated-token lengths. TP=8.

OCS Type	Reconfig. delay (ms)	Radix ports
RotorNet (InFocus) [48]	0.01	128
3D MEMS (Calient) [54]	10	320
Piezo (Polatis) [27]	25	576
Liquid crystal (Coherent) [2, 32]	100	512
Robotic (Telescent) [63]	120000	1008

Table 2: Representative reconfiguration delays and radix port counts for commodity OCS technologies.

A Cost of KV-Cache Migration vs. Recomputation

We present an example for KV-cache rebuilding overhead in Qwen-32B, including communication and synchronization for direct transfer, as well as forward-pass compute for recomputation, in Figure 19. In general, direct transfer is more efficient for larger KV cache sizes (e.g., more generated tokens and/or larger batch sizes), while recomputation becomes favorable when the cache is smaller or communication bandwidth is a limiting factor. It is worth noting that this example assumes a single NIC with an aggregated bandwidth of 200 Gbps for KV-state transfer. In practical scenarios, where the layout between instances allows for multiple NICs, direct transfer can achieve significantly higher speeds.

Using profiled cost curves under various settings, our runtime dynamically selects the lower-cost option for each reconfiguration event.

B OCS Reconfiguration Time

Table 2 summarizes the reconfiguration delays and radix port counts of various commodity OCS technologies.

C Model Configuration Summary

Table 3 summarizes the key architectural hyperparameters of the Qwen variants used in this paper. We report the training-time parallelism configurations used in our experiments. For Qwen-72B training, we primarily use TP=8, PP=2, and CP=3,

Model	Total	d_{model}	Layers	FFN intermediate	# Query heads	# KV heads
Qwen2.5-14B	14.7B	5120	48	13824	40	8
Qwen2.5-32B	32.5B	5120	64	27648	40	8
Qwen2-57B-A14B (MoE)	57.41B	3584	28	2560×64	28	4
Qwen2.5-72B	72.7B	8192	80	29568	64	8
Qwen3-235B-A22B (MoE)	235B	4096	94	1536×128	64	4

Table 3: Model configuration summary. For MoE, the FFN intermediate is written as (expert dim) \times (num experts).

and scale DP accordingly. For Qwen-57B-A14B training, we primarily use TP=4 and EP=16, and scale DP accordingly.

D OCS Port Allocation

This appendix describes OrchestrRL’s OCS port/circuit allocation. We present (i) a tier-agnostic allocation abstraction shared by OCS-Agg and OCS-Core, and (ii) a bounded-time greedy allocator for circuit allocation.

Agg/Core relationship. In each period, OrchestrRL produces both an OCS-Agg plan (within each PoD, including ToR–uplink lift/drop) and an OCS-Core plan (across PoDs). The two tiers are coupled: inter-PoD Core capacity incident to a PoD must be supportable by that PoD’s available boundary uplinks and the corresponding lift/drop access capacity. We therefore accept and commit a plan only if the resulting Agg/Core allocations are jointly feasible under the current fabric state.

D.1 Problem Abstraction

For each upcoming communication period, OrchestrRL produces a sparse directed demand matrix $\{D_{u \rightarrow v}\}_{u,v \in V, u \neq v}$, where $D_{u \rightarrow v}$ is the predicted bytes sent from endpoint u to v during the period. For OCS-Core, endpoints are PoDs. For OCS-Agg, we use a ToR-centric view: each PoD is solved independently, and V includes the PoD’s ToRs as well as PoD-boundary uplink endpoints (i.e., the attachment points to OCS-Core). This abstraction covers both intra-PoD ToR–ToR demands and inter-PoD access demands (ToR–uplink) that lift/drop traffic to/from OCS-Core. In practice, demands are represented sparsely as a directed edge set $E_{\rightarrow} \subseteq V \times V$ (e.g., after AGGREGATEDEMAND); for $(u, v) \notin E_{\rightarrow}$, we treat $D_{u \rightarrow v} = 0$. (When constructing undirected candidate pairs, the implementation enumerates from the sparse demanded edges and their reverses, rather than all $|V|^2$ pairs.)

A circuit is a discrete capacity unit between an endpoint pair. Each circuit is full duplex and provides line rate B_{link} in each direction. Let $\text{deg}(v)$ denote the number of allocatable OCS ports at endpoint v after applying port reservations.

Decision variables. We allocate integer circuit multiplicities $c_{uv} \geq 0$ over endpoint pairs, where $c_{uv} = c_{vu}$ denotes the number of parallel full-duplex circuits between endpoints u and v .

Port budget constraint. Each circuit consumes one port at each endpoint, hence:

$$\sum_{u:u \neq v} c_{uv} \leq \deg(v) \quad \forall v \in V. \quad (6)$$

Template scope. The selected topology template tpl determines which pairs are OCS-eligible via $\text{ELIGIBLE}(tpl, u, v)$ (and may additionally impose per-pair or role constraints). This appendix focuses on allocating c_{uv} on eligible pairs under the port budget (i.e., we implicitly enforce $c_{uv} = 0$ when $\neg \text{ELIGIBLE}(tpl, u, v)$).

D.2 Greedy Circuit Allocation

Exact optimization over integer circuit multiplicities is expensive at scale, so OrchestrRL uses a greedy allocator. The algorithm allocates circuits one-by-one until no demanded eligible pair has free ports at both endpoints. The number of iterations is bounded by $\frac{1}{2} \sum_{v \in V} \deg(v)$; moreover, the demand graph is usually sparse after AGGREGATEDEMAND .

Given directed demands but full-duplex circuits, we score bottlenecks at the endpoint-pair granularity. For each eligible pair $\{u, v\}$, define a completion-time proxy:

$$T^{\text{pair}}[u, v] = \begin{cases} \max\left(\frac{D_{u \rightarrow v}}{c_{uv} B_{\text{link}}}, \frac{D_{v \rightarrow u}}{c_{uv} B_{\text{link}}}\right), & c_{uv} > 0, \\ +\infty, & c_{uv} = 0 \wedge (D_{u \rightarrow v} + D_{v \rightarrow u} > 0), \\ 0, & c_{uv} = 0 \wedge (D_{u \rightarrow v} + D_{v \rightarrow u} = 0). \end{cases} \quad (7)$$

Intuitively, T^{pair} approximates the time to serve the slower direction on the pair using the currently allocated parallel circuits; a demanded pair with zero circuits is treated as an infinite bottleneck.

At each step, ALLOCATECIRCUITS (Algorithm 3) selects the demanded eligible pair with the largest T^{pair} among those with at least one free port on both endpoints, and allocates one additional circuit to that pair. When multiple pairs have $T^{\text{pair}} = +\infty$, ties are broken by the larger directional demand $\max(D_{u \rightarrow v}, D_{v \rightarrow u})$. For certain templates (e.g., bipartite structures), the implementation may optionally add a utilization-aware tie-breaker to reduce port monopolization by hot endpoints and preserve feasible matchings.

After allocation, the system checks hard feasibility constraints (e.g., device/template constraints and that the planned ports remain free at commit time) before committing the plan. It also enforces Core-Agg consistency for inter-PoD traffic: the planned OCS-Core capacity must be supportable by OCS-Agg ToR-uplink access capacity in the corresponding source and destination PoDs.

Algorithm 3 ALLOCATECIRCUITS (pair bottleneck greedy on OCS-eligible pairs)

```

1: procedure  $\text{ALLOCATECIRCUITS}(tpl, G, S)$ 
2:    $(V, E_{\rightarrow}, D_{\rightarrow}) \leftarrow G$ 
3:    $(\deg(\cdot), B_{\text{link}}) \leftarrow S$ 
4:    $C \leftarrow \mathbf{0}$  ▷ symmetric (full-duplex) circuit multiplicities
5:   for all  $v \in V$  do
6:      $p[v] \leftarrow \deg(v)$ 
7:   while true do
8:      $\mathcal{P} \leftarrow \{\{u, v\} \mid u \neq v \wedge \text{ELIGIBLE}(tpl, u, v) \wedge p[u] > 0 \wedge p[v] > 0 \wedge (D_{\rightarrow}(u, v) + D_{\rightarrow}(v, u) > 0)\}$ 
9:     if  $\mathcal{P} = \emptyset$  then
10:      break
11:      ▷ Pick pair with max PAIRTIME; break ties by MAXDIRDEMAND.
12:       $\{u^*, v^*\} \leftarrow \arg \max_{\{u, v\} \in \mathcal{P}} \left( \text{PAIRTIME}(u, v, C, D_{\rightarrow}, B_{\text{link}}), \right.$ 
13:         $\text{MAXDIRDEMAND}(u, v, D_{\rightarrow})$ 
14:         $\left. \right)$ 
15:       $a \leftarrow \min(u^*, v^*); b \leftarrow \max(u^*, v^*)$ 
16:       $C[a][b] \leftarrow C[a][b] + 1; C[b][a] \leftarrow C[b][a] + 1$ 
17:       $p[a] \leftarrow p[a] - 1; p[b] \leftarrow p[b] - 1$ 
18:      return  $C$ 
19: function  $\text{PAIRTIME}(u, v, C, D_{\rightarrow}, B_{\text{link}})$ 
20:    $c \leftarrow C[u][v]$ 
21:    $d_{uv} \leftarrow D_{\rightarrow}(u, v); d_{vu} \leftarrow D_{\rightarrow}(v, u)$ 
22:   if  $d_{uv} + d_{vu} = 0$  then
23:     return  $0$ 
24:   else if  $c = 0$  then
25:     return  $+\infty$ 
26:   else
27:     return  $\max(d_{uv}, d_{vu}) / (c \cdot B_{\text{link}})$ 
28: function  $\text{MAXDIRDEMAND}(u, v, D_{\rightarrow})$ 
29:   return  $\max(D_{\rightarrow}(u, v), D_{\rightarrow}(v, u))$ 

```

E Tree-Style Broadcast for Weight Synchronization

This appendix describes RFabric’s two-level, circuit-scheduled broadcast for disseminating weight shards. Each shard is disseminated via its own tree; over many shards, the system materializes a temporary dissemination *forest*, and tears it down after synchronization completes.

Weight synchronization disseminates a large parameter shard from Train endpoints that hold the shard to all Gen endpoints that require it. A naive one-to-all design (each Train sender directly to every Gen receiver) scales poorly because inter-PoD transfers must traverse the PoD boundary, where Core-facing OCS ports are limited and can easily become hotspots. RFabric therefore materializes a temporary *two-level dissemination overlay* with ample scheduling slack: Phase A seeds a small set of Gen receivers across PoDs using OCS-Core; Phase B completes intra-PoD fanout inside each destination PoD.

Endpoints and PoD-boundary concurrency budgets. Endpoints are GPUs/server NICs (ranks); let $\text{POD}(x)$ denote the PoD containing endpoint x . OCS-Core constraints are enforced at the *PoD boundary*: each PoD p has a budget d_p

that caps the number of *concurrently active inter-PoD circuits* incident to p (counting one unit at both the source and destination PoDs). Equivalently, d_p captures the scarce boundary-facing OCS-Core port capacity available for simultaneous use. Gateway endpoints (when used) only affect which endpoints terminate boundary-facing circuits; budgets are still accounted per PoD. In addition, realizing a Phase A inter-PoD OCS-Core transfer may require intra-PoD connectivity to reach the boundary-facing uplinks (e.g., via OCS-Agg circuits between ToRs and uplinks), in both the Train source PoD and the Gen destination PoD.

E.1 Phase A: Cross-PoD Seeding on OCS-Core

Senders, destinations, and seeds. Let \mathcal{S} be the set of Train-side sender candidates that hold the shard (e.g., shard owners or replicas). Let \mathcal{D} be the set of Gen endpoints that ultimately need the shard. Phase A delivers the shard only to a small set of *seed receivers* $\mathcal{R} \subseteq \mathcal{D}$ (typically a constant number per destination PoD); Phase B then fans out from seeds to all remaining endpoints within each destination PoD, avoiding redundant cross-PoD replication.

Overlay construction and budget-aware scheduling. Phase A constructs an inter-PoD overlay on endpoints, in which each scheduled edge (u, v) satisfies $\text{POD}(u) \neq \text{POD}(v)$. We activate a subset of roots $\mathcal{S}_{\text{act}} \subseteq \mathcal{S}$ and assign each seed to exactly one active root: $\mathcal{R} = \bigsqcup_{s \in \mathcal{S}_{\text{act}}} \mathcal{R}_s$. Because PoD-boundary budgets bound *concurrency*, Phase A may run in multiple *waves*. Let \mathcal{E}_t be the set of inter-PoD edges active in wave t , and let $c_{uv}^{(t)} \geq 1$ be the number of circuits allocated to $(u, v) \in \mathcal{E}_t$. Feasibility requires, for every PoD p and wave t ,

$$\sum_{(u,v) \in \mathcal{E}_t: \text{POD}(u)=p} c_{uv}^{(t)} + \sum_{(u,v) \in \mathcal{E}_t: \text{POD}(v)=p} c_{uv}^{(t)} \leq d_p.$$

Circuit allocation and completion time. Each scheduled inter-PoD edge (u, v) is realized by $c_{uv}^{(t)}$ parallel point-to-point circuits of line rate B_{link} . Let $S_{uv}^{(t)}$ be the data volume sent on (u, v) in wave t (e.g., shard chunks). Assuming circuit-level isolation and sufficiently large chunks, the wave completion time is well-approximated by the slowest edge:

$$T_A^{(t)} \approx \max_{(u,v) \in \mathcal{E}_t} \frac{S_{uv}^{(t)}}{c_{uv}^{(t)} \cdot B_{\text{link}}}, \quad T_A \approx \sum_t T_A^{(t)}.$$

Given a fixed eligible edge set (the Phase A overlay), RFabric allocates at least one circuit per scheduled edge and greedily adds circuits to equalize per-edge bottlenecks while respecting the per-PoD incidence budgets $\{d_p\}$ (similar in spirit to the bottleneck-equalization heuristic in Appendix D).

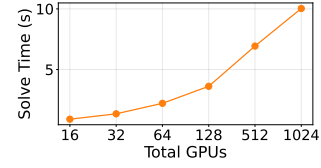


Figure 20: Optimization solving time across GPU scales. The total number of requests is set to $16 \times \# \text{GPUs}$.

Link Bandwidth	Transceiver (\$)	NIC (\$)	Elec. Switch Port (\$)	OCS Port (\$)	Patch Panel Port (\$)	Fiber Cable (\$)
100 Gbps	249 [17]	736 [25]	215 [19]	350 [15, 47]	100 [63]	25 [14]
200 Gbps	499 [18]	1,291 [22]	876 [26]	350 [15, 47]	100 [63]	45 [20]
400 Gbps	799 [11]	1,710 [23]	1,392 [16]	350 [15, 47]	100 [63]	65 [21]
800 Gbps	1,599 [12]	2,347 [24]	1,731 [13]	350 [15, 47]	100 [63]	92 [28]

Table 4: Price of Network Components.

E.2 Phase B: Intra-PoD Fanout on OCS-Agg

Once a seed in a destination PoD receives the shard, it disseminates it to the remaining Gen ranks within the same PoD. To accelerate cross-rack fanout and avoid bottlenecks at a single root NIC, rack uplink, or ToR, RFabric may materialize intra-PoD OCS-Agg circuits (or use rack-local EPS when sufficient). This allows Phase A to reduce cross-PoD boundary occupancy by seeding only \mathcal{R} . Within each destination PoD, RFabric schedules an intra-PoD dissemination tree—or multiple trees rooted at different seeds—so that each seed serves only a fraction of receivers.

F Optimization Solving Time

Figure 20 reports the solving time of the optimization problem in our compute scheduler across different GPU scales for Qwen-57B-MoE model. Even at a scale of 1024 GPUs with a large request volume, the solver finishes in under 11 s, which can be largely overlapped with phases such as weight synchronization. Moreover, during a generation step, the number of active requests naturally decreases as requests complete; thus, for the same GPU scale, the optimization solving time typically decreases accordingly.

G Network Component Price

Table 4 summarizes indicative prices for different network components, compiled from a search of recent market listings and publicly available pricing information. These values are used as baseline inputs for our cost comparison and do not represent vendor quotes.

H Failure Handling

We evaluate RFabric’s resiliency to link failures using Qwen2-57B-MoE across different RL stages, considering failures on

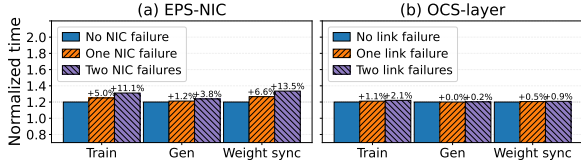


Figure 21: Impact of link failures on end-to-end time (normalized) across RL stages for Qwen2-57B-MoE. We inject one or two failures on (a) NIC–EPS links and (b) OCS-layer links, and report the normalized Train, Gen, and Weight Sync time.

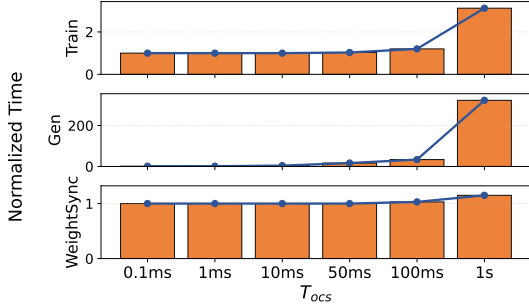


Figure 22: Sensitivity to OCS update time under fine-grained reconfiguration across RL stages.

the NIC–EPS link and on links in the OCS layer. Figure 21 shows that a NIC–EPS link failure has a noticeable impact on communication-intensive stages: Train slows down by 5.0% (one failure) and 11.1% (two failures), while Weight Sync degrades by 6.6% and 13.5%, respectively. This is because a NIC–EPS failure forces the affected GPU to reroute its traffic through the scale-up domain (e.g., NVLink/NVSwitch) to a healthy NIC, creating additional intra-node hops and oversubscribing the remaining NICs.

In contrast, Gen is less sensitive (only 1.2% and 3.8% slow-down) because it runs in AFD mode, where communication overhead can be largely overlapped with computation.

Failures in the OCS layer have a much smaller impact: Train increases by only 1.1% and 2.1% under one and two link failures, and Weight Sync by 0.5% and 0.9%, while Gen remains nearly unchanged (0.0% and 0.2%). This is because OCS-layer failures can often be masked by multi-path routing (e.g., ECMP), whereas a NIC–EPS failure directly reduces the available bandwidth at the endpoint and concentrates traffic on fewer NICs.

I Sensitivity Analysis

Sensitivity to T_{ocs} . We sweep T_{ocs} over representative values and report the normalized stage time of Train, Gen, and Weight Sync for Qwen-235B-A22B (Figure 22). We assume fine-grained reconfiguration in each stage—in contrast

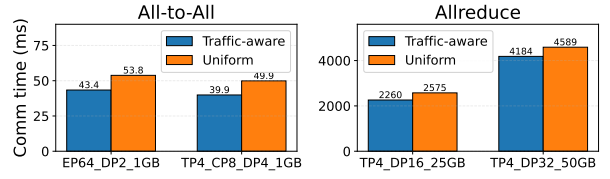


Figure 23: Collective performance of RFabric under traffic-aware allocation versus uniform allocation with 200 Gbps links. Labels denote the parallelism configuration, and sizes (1/25/50 GB) are per-rank message sizes. All-to-all runs over the EP/CP domain, while allreduce runs over the DP domain.

to our stage-dependent adaptive granularity—including in-execution updates when communication patterns shift (e.g., during AFD in Gen, MoE transitions from cross-server all-to-all to M2N back to attention, triggering a reconfiguration). Sensitivity is stage-dependent and matches the slack distributions in §2. Train degrades gradually as T_{ocs} grows because reduced compute slack can no longer hide reconfiguration; it remains stable for $T_{ocs} \leq 100$ ms. Gen is highly sensitive: even millisecond-scale reconfiguration can become a bottleneck due to limited overlap slack, inflating latency by 4–325 \times . Weight Sync is minimally affected over practical ranges because it has ample slack and the completion time is nearly unchanged.

Traffic-aware allocation vs. uniform splitting. Figure 23 shows that RFabric’s traffic-aware allocation outperforms uniform splitting across the evaluated collectives and configurations. For all-to-all, traffic-aware reduces communication time by 19.3% on EP64_DP2_1GB and 20.0% on TP4_CP8_DP4_1GB. For allreduce, it reduces communication time by 12.1% on TP4_DP16_25GB and 8.8% on TP4_DP32_50GB. Uniform splitting spreads scarce OCS ports (and thus circuit capacity) evenly across endpoints, which can over-provision low-demand pairs while leaving hotspots under-provisioned. In contrast, traffic-aware allocation concentrates circuits on high-demand pairs and dominant bottlenecks, improving collective communication performance.